High Precision Sensorless Control of Rotor Mechanical Position based on Cross Correction of Dual Air Gap Information

Yukun Lin, Ronggang Ni, *Senior Member*, *IEEE*, Shengming Yang, and Qingwen Deng

***Abstract*—Position sensors are indispensable in robotic joint servo systems for acquiring mechanical positions, yet their installation inevitably occupies an axial space and increases system complexity, limiting their applicability in compact robot design where spatial constraints and integration efficiency are critical. Sensorless control reduces mechanical and circuit complexity through hardware simplification, but inherently estimates only the electrical instead of mechanical rotor position information, thus remaining constrained in robot joint control applications. Based on the previously proposed dual-gap dual-pole composite machine (DDCM), this paper systematically analyzes the causes of mechanical position estimation errors and proposes a correction method that utilizes a correction coefficient to reduce these errors and enhance estimation accuracy. Furthermore, this paper derives the applicability constraints of the proposed scheme, demonstrating that its requirements for electrical angle position errors are not stringent, thus enabling wide applicability in conventional sensorless control scenarios. The effectiveness of the proposed method is verified by conducting experiments on a 0.75 kW prototype.**

***Index Terms*—Dual-gap dual-pole composite machine (DDCM), Electrical angle position errors, Mechanical position estimation errors, Sensorless control.**

I. Introduction

In recent years, high-end equipment has been developing rapidly with the continuous upgrading of the manufacturing industry, where position servo drive is commonly a basic requirement [1]-[3]. The mechanical rotor position (also known as absolute rotor position) of electric machines is typically measured by dedicated sensors such as encoders (incremental or absolute) and resolvers [4]-[5]. Incremental encoders solely measure relative rotor positions, necessitating an additional reference signal for absolute rotor position determination, and lose absolute position information upon power-off [6]-[7]. Absolute encoders can detect the rotor's absolute position immediately upon system power-up; however, they present higher implementation costs and signal transmission complexity compared to incremental encoders [8]-[9]. By contrast, resolvers exhibit strong interference immunity. Among these, single-pole-pair resolvers autonomously detect the rotor's mechanical position upon energization, yet their detection accuracy remains relatively low [10].

Regardless of the selection, the installation of position sensors inherently occupies an axial space, not only increasing mechanical complexity but also compromising system power density and operational reliability [11]-[12]. Such limitations motivate the widespread utilization of sensorless techniques in speed closed-loop control systems, owing to their cost-effectiveness and enhanced reliability [13]-[14]. However, due to the periodic symmetry of the motor's magnetic circuit structure, sensorless control for multi-pole motors can only resolve the rotor electrical angle. As there exists a one-to-multiple mapping between the electrical angle and mechanical position, the rotor's absolute mechanical position is unobservable.

In response to the issue that sensorless control can only estimate the rotor electrical angle, Kwon *et al*. [15]-[17] have attempted to design motors with structurally asymmetric configurations to achieve sensorless mechanical angle estimation. Nevertheless, this asymmetric design introduces challenges, including increased winding inductance and back electromotive force (back-EMF) harmonic distortion, necessitating further structural optimization.

Without introducing mechanical asymmetry, [18] proposes a dual-gap dual-pole composite machine (DDCM) topology with a dual-stator single-rotor configuration, along with conventional sensorless techniques for mechanical position estimation. As shown in Fig. 1, this structure can combine any two motors with different pole-pair combinations in a variety of topological forms, offering more options for motor design.

When conventional sensorless control techniques are employed for position estimation in DDCM, electrical angle errors inevitably occur. Both injection methods based on rotor saliency detection at low speeds [19] and model-based methods relying on back-EMF observation at high speeds [20] inherently contain alternating current (AC) and direct current

Manuscript received June 25, 2025; revised September 20, 2025; accepted October 09, 2025. Date of publication December 25, 2025; Date of current version November 20, 2025.

This work was supported in part by the National Natural Science Foundation of China under Grants 52277057 and U22A20217, and in part by the Shandong Youth Innovation Team under Grant 2022KJ150.

Yukun Lin, Ronggang Ni, Shengming Yang, and Qingwen Deng are with the School of Electrical Engineering, Qingdao University, Qingdao 266071, China (e-mail: linyukun@qdu.edu.cn; ron4ni@163.com; 2021020639@qdu.edu.cn; dengqingwen@qdu.edu.cn).

(*Corresponding author*: *Ronggang Ni*)

Digital Object Identifier 10.30941/CESTEMS.2025.00032

(DC) components in the position estimation error. For high-frequency injection techniques, the DC component of the error is usually difficult to eliminate due to the influence of quadrature-axis armature reaction [21]-[22]. The sliding mode control inherently causes the current observation error to fluctuate near the sliding mode surface, which leads to high-frequency vibration of the position error [23]-[24]. While AC components can be suppressed through observer optimization, temperature-dependent resistance variations [25] and q-axis current-dependent inductance variations [26] during motor operation also induce DC errors.

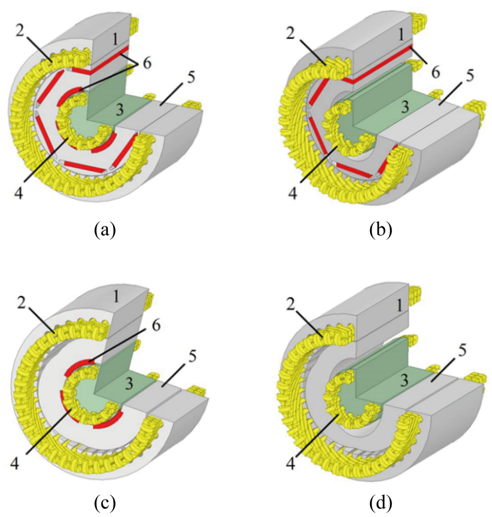

1-outer stator; 2-outer winding; 3-inner stator; 4-inner winding; 5-rotor; 6-permanent magnet

Fig. 1. DDCM of different topologies. (a) Permanent magnet synchronous motor (PMSMs) for both air gaps. (b) PMSM for the outer and reluctance machine (RM) for the inner air gaps. (c) RM for the outer and PMSM for the inner air gaps. (d) RMs for both air gaps.

Despite significant advantages from its unique structure, the DDCM introduces new challenges. The DDCM features dual air gaps, and the mechanical rotor position is acquired through the demodulation of signals from both air gaps. When considering the electrical angle errors in the inner and outer air gaps, the mechanical position estimation error is inevitably affected by the combined influence of the electrical angle estimation errors present in both air gaps. Analysis of subsequent sections indicates that under extreme operating conditions, these position errors may exceed the electrical angle error of either air gap.

To solve this issue, this paper proposes the variable dual-pole mechanical angle deviation for correcting the original mechanical position solution equation. The method calibrates mechanical position errors to inner or outer air-gap electrical angle errors divided by respective pole-pair numbers, notably enhancing position accuracy. It also derives the correction method's constraints. Comparative studies show its low sensitivity to electrical angle deviations, enabling effective correction even under large errors and broad applicability in conventional sensorless control.

The paper is organized as follows. Section II introduces the observation principle of DDCM mechanical position and further discusses the factors affecting mechanical position errors. Section III proposes the variable dual-pole mechanical angle deviation and performs subsequent mechanical position error correction based on this variable, while discussing the necessary calibration conditions to be satisfied. Section IV carries out an experimental validation in a 0.75 kW DDCM to verify the effectiveness of the correction method. Finally, Section V concludes the paper.

II. Mechanical Position Observation Principle and Causes of Position Error

A. *Principles of Mechanical Position Observation*

When the specific pole-pairs ratio is satisfied, the mechanical position of the DDCM is obtained as (1):

$$\theta_{\mathrm{m}} = \pm\left(m_1\theta_{\mathrm{e1}} - m_2\theta_{\mathrm{e2}}\right) \tag{1}$$

where θ_{m} is the observed mechanical position of the rotor. θ_{e1}, θ_{e2} are the electrical angles of the outer and the inner air gaps, respectively, with their relationship given by (2):

$$\begin{cases}\theta_{\mathrm{e1}} = p_1\theta_{\mathrm{m}} \\ \theta_{\mathrm{e2}} = p_2\theta_{\mathrm{m}}\end{cases} \tag{2}$$

Take positive integers m_1 and m_2 such that (3) holds:

$$m_1 p_1 - m_2 p_2 = \pm 1 \tag{3}$$

where p_1 and p_2 are the pole-pairs of the outer and the inner air gaps, and they are mutually prime. The right side of the equal sign of (3) is usually taken as a positive sign for the sake of simplicity, although there is no essential difference between the positive and negative signs. The combination of p_1 and p_2 is more important than the arrangement.

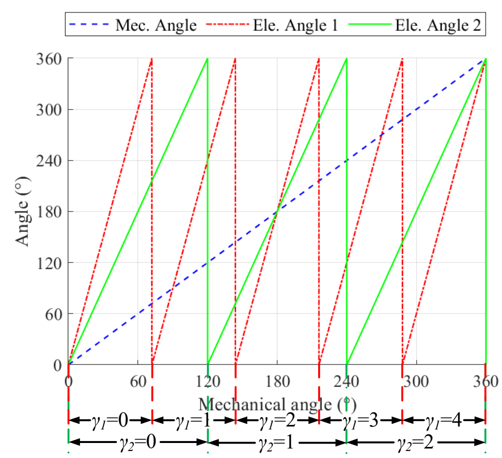

Fig. 2. The relationship between mechanical angle, inner, and outer air gap electrical angle and rounding.

γ_1 and γ_2 are defined as the product of the number of dual air gap pole-pairs and the mechanical angle, and then the value is rounded to the nearest integer multiple of 2π, that is expressed as (4):

$$\begin{cases}\gamma_1 = \operatorname{int}\left[p_1\theta_{\mathrm{m}} / 2\pi\right] \\ \gamma_2 = \operatorname{int}\left[p_2\theta_{\mathrm{m}} / 2\pi\right]\end{cases} \tag{4}$$

Taking p_1=5 and p_2=3 as an example, the relationship of (4) in the complete mechanical period is shown in Fig. 2. The blue line indicates the mechanical position, the dashed red line indicates the electrical position of the outer air gap, and the solid green line indicates the electrical position of the inner air gap.

Under sensorless operation, the estimated mechanical speed obtained by dividing the electrical angle velocity of either air gap by its respective pole-pair number is fed back to the speed loop. Following the speed loop, torque allocation is performed between the inner and outer motors. The control block diagram of the entire system is presented in Fig. 3.

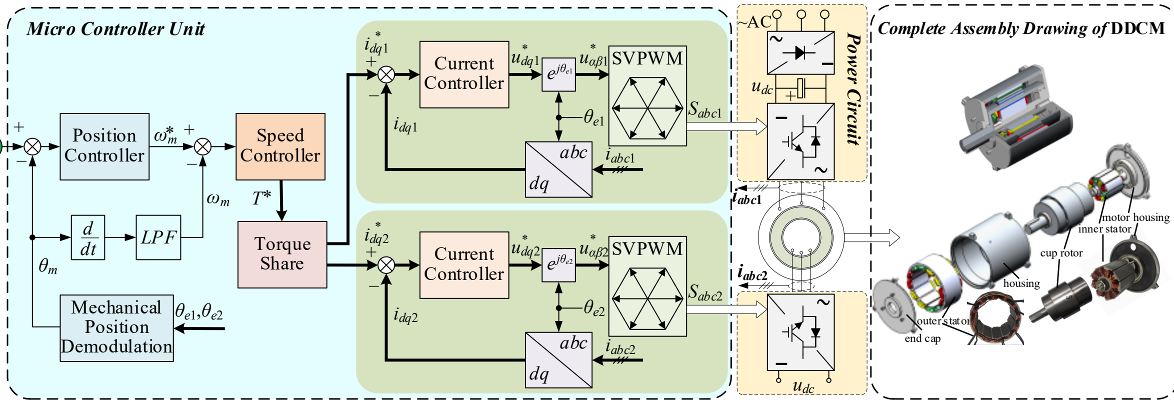

Fig. 3. DDCM control system block diagram.

B. Causes of Mechanical Positioning Errors

Conventional sensorless control inherently incurs electrical angle errors, while the aforementioned mechanical position estimation method does not account for this error. When considering the electrical angle errors in both inner and outer air gaps, the observed mechanical position can be described as (5):

$$\begin{aligned}\hat{\theta}_{\mathrm{m}} &= m_1\hat{\theta}_{\mathrm{e1}} - m_2\hat{\theta}_{\mathrm{e2}} \\ &= m_1\left(\theta_{\mathrm{e1}} + \tilde{\theta}_{\mathrm{e1}}\right) - m_2\left(\theta_{\mathrm{e2}} + \tilde{\theta}_{\mathrm{e2}}\right) \\ &= \left(m_1 p_1 - m_2 p_2\right)\theta_{\mathrm{m}} + \left(m_1\tilde{\theta}_{\mathrm{e1}} - m_2\tilde{\theta}_{\mathrm{e2}}\right) \\ &= \theta_{\mathrm{m}} + \left(m_1\tilde{\theta}_{\mathrm{e1}} - m_2\tilde{\theta}_{\mathrm{e2}}\right)\end{aligned} \tag{5}$$

where $\hat{\theta}_{\mathrm{e1}}$ and $\hat{\theta}_{\mathrm{e2}}$ are the estimated electrical angles of the outer and inner air gaps considering errors, $\tilde{\theta}_{\mathrm{e1}}$ and $\tilde{\theta}_{\mathrm{e2}}$ are the observed electrical angle errors of the outer and the inner air gaps.

Therefore, the observed mechanical position error can be obtained as (6):

$$\tilde{\theta}_{\mathrm{m}} = \hat{\theta}_{\mathrm{m}} - \theta_{\mathrm{m}} = m_1\tilde{\theta}_{\mathrm{e1}} - m_2\tilde{\theta}_{\mathrm{e2}} \tag{6}$$

From (6), it can be seen that the observed mechanical position error is determined by m_1 and m_2, and the inner and the outer air gaps' electric angle error. According to (3), m_1 and m_2 are determined by p_1 and p_2. Therefore, the factors affecting mechanical position error are divided into the following three.

1) Pole-pair combination of outer and inner air gaps. Taking p_1=5, p_2=4 and p_1=5, p_2=3 as an example, using the positive value of (3), Fig. 4 shows mechanical position errors of −8° (Point A) and −20° (Point B) under fixed electrical angle errors ($\tilde{\theta}_{\mathrm{e1}}$ =−4°, $\tilde{\theta}_{\mathrm{e2}}$ =4°). This demonstrates that identical electrical angle errors under different pole-pair numbers result in distinct mechanical rotor position errors.

2) Phase of electrical angle errors in the inner and outer air gaps. As indicated in (6), the observed mechanical position error varies with the phase difference of the electrical angle error. Taking p_1=5 and p_2=3 as an example, m_1=2 and m_2=3 are derived from (3). When both $\tilde{\theta}_{\mathrm{e1}}$ and $\tilde{\theta}_{\mathrm{e2}}$ are 4°, the observed mechanical position error is −4° (Point C in Fig. 4). However, when $\tilde{\theta}_{\mathrm{e1}}$ is 4° and $\tilde{\theta}_{\mathrm{e2}}$ is −4°, the observed mechanical position error reaches 20° (Point D in Fig. 4).

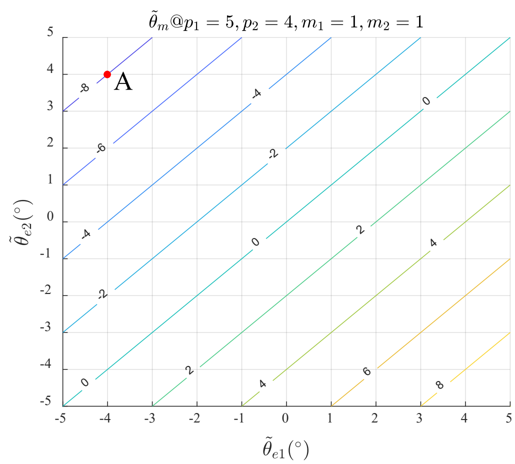

(a)

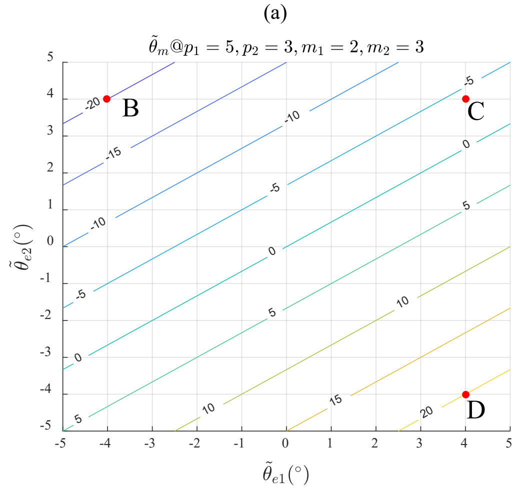

(b)

Fig. 4. Solving mechanical position errors under the coordination of different pole-pairs. (a) p_1=5, p_2=4. (b) p_1=5, p_2=3.

3) m_x takes different values. Taking p_1=5 and p_2=3 as an example, both m_1=2, m_2=3 and m_1=−1, m_2=−2 satisfy condition (3). When $\tilde{\theta}_{\mathrm{e}1}$ is set to 10° and $\tilde{\theta}_{\mathrm{e}2}$ is set to −10°, the calculated mechanical position errors are 50° and −10°, respectively. This demonstrates that the selection of m values directly impacts the magnitude of the calculated mechanical position errors.

The analysis indicates that mechanical position errors, influenced by multiple factors, exhibit instability in calculation, necessitating a novel calibration method for error reduction.

III. Mechanical Position Error Correction

A. Dual Pole Mechanical Angle Deviation

Prior analysis indicates that the solved mechanical position error is influenced by multiple factors. To minimize this error, position correction is required.

The rotor mechanical angle position satisfies the ratio relationship between the electrical angle position and the pole-pair number; thus, it is desired to suppress the rotor mechanical angle error to the ratio of the electrical angle position error to the pole-pair number. The dual pole mechanical angle deviation θ_{md} is thus defined as (7):

$$\begin{aligned}\theta_{\mathrm{md}} &= \frac{\theta_{\mathrm{e}1}}{p_1} - \frac{\theta_{\mathrm{e}2}}{p_2} \\ &= \frac{\mathrm{mod}\left(p_1\theta_{\mathrm{m}}, 2\pi\right)}{p_1} - \frac{\mathrm{mod}\left(p_2\theta_{\mathrm{m}}, 2\pi\right)}{p_2} \\ &= \frac{\left(p_1\theta_{\mathrm{m}} - \gamma_1 \cdot 2\pi\right)}{p_1} - \frac{\left(p_2\theta_{\mathrm{m}} - \gamma_2 \cdot 2\pi\right)}{p_2} \\ &= \left(\frac{\gamma_2}{p_2} - \frac{\gamma_1}{p_1}\right) \cdot 2\pi\end{aligned} \tag{7}$$

It can be obtained from (7) that the value of θ_{md} is related to the number of inner and outer air gap poles and the number of rounding γ_1 and γ_2. Within the defined interval γ_1 and γ_2, θ_{md} remains constant. When different pole-pair numbers are employed, the value of θ_{md} throughout the complete mechanical cycle is depicted in Fig. 5.

When the electrical angle error is considered, the observed value of θ_{md} is described as (8):

$$\begin{aligned}\hat{\theta}_{\mathrm{md}} &= \frac{\hat{\theta}_{\mathrm{e}1}}{p_1} - \frac{\hat{\theta}_{\mathrm{e}2}}{p_2} \\ &= \left(\frac{\gamma_2}{p_2} - \frac{\gamma_1}{p_1}\right) \cdot 2\pi + \left(\frac{\tilde{\theta}_{\mathrm{e}1}}{p_1} - \frac{\tilde{\theta}_{\mathrm{e}2}}{p_2}\right)\end{aligned} \tag{8}$$

From (8), it can be seen that when the electrical angle error is considered, the electrical position is shifted, and the number of integer-rounding operations for parameters γ_1 and γ_2 undergoes variations.

When electrical angle errors are neglected, the rounding counts for the outer and the inner air gaps are given by γ_1= p_1−1 and γ_2=p_2−1, respectively, as depicted in Fig. 2. When the outer air gap $\tilde{\theta}_{\mathrm{e}1}$ is ahead of the inner air gap $\tilde{\theta}_{\mathrm{e}2}$, the outer air gap undergoes an additional integer-rounding operation. In this case, γ_1=p_1 and γ_2=p_2−1. When the inner air gap $\tilde{\theta}_{\mathrm{e}2}$ is advanced relative to the external air gap $\tilde{\theta}_{\mathrm{e}1}$, the outer air gap undergoes an additional integer-rounding operation. In this case γ_1=p_1−1, γ_2=p_2.

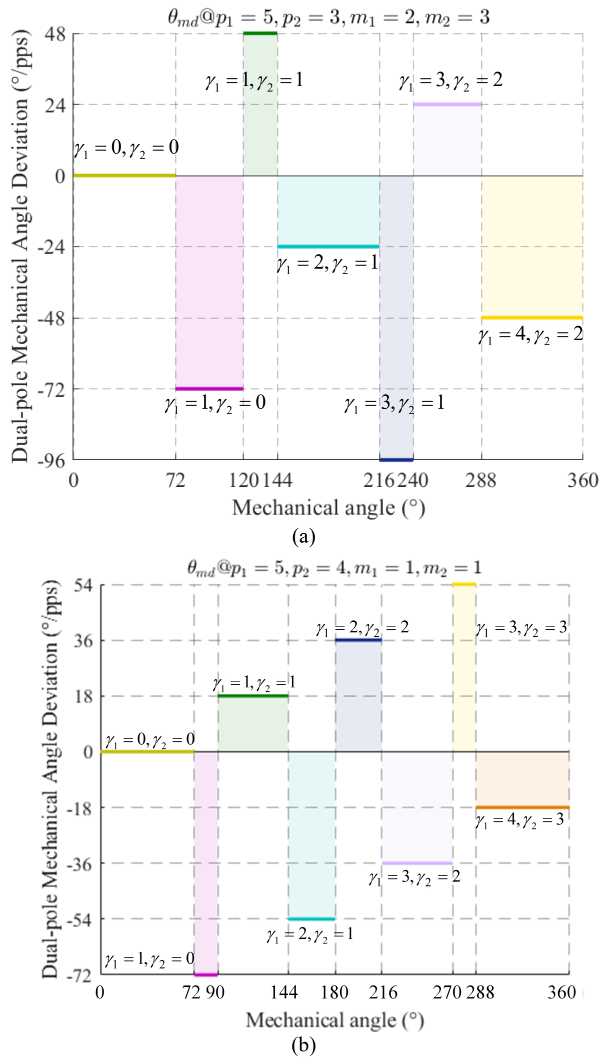

Fig. 5. The value of θ_{md} in the complete mechanical period under different pole-pair ratios. (a) p_1=5, p_2=3. (b) p_1=5, p_2=4.

Taking p_1=5 and p_2=3 as an example, m_1=2 and m_2=3 can be obtained from (3). When taking into account the electrical angle position error, the specific value of θ_{md} is denoted as θ'_{md}. For convenient comparison, the phases of the electrical angle errors in the inner and outer air gaps differ by 60°. When $\tilde{\theta}_{\mathrm{e}1}$ (outer air gap) leads, θ'_{md}=−120° is calculated at the end of the mechanical cycle, as shown in Fig. 6(a); when $\tilde{\theta}_{\mathrm{e}2}$ (inner air gap) leads, θ'_{md}=72° is calculated at the end of the mechanical cycle, as shown in Fig. 6(b).

From the above analysis, it can be seen that θ_{md} and γ_1, γ_2 will be divided into a set of different discrete values in the complete mechanical cycle with the change of mechanical position. When the electrical angle error exists, the set elements will increase. But each element is still different.

Therefore, the value range of γ_1 and γ_2 must be in the above set. Half of the interval value between each θ_{md} is defined as the tolerance. The observed mechanical position error can be corrected by judging θ_{md}.

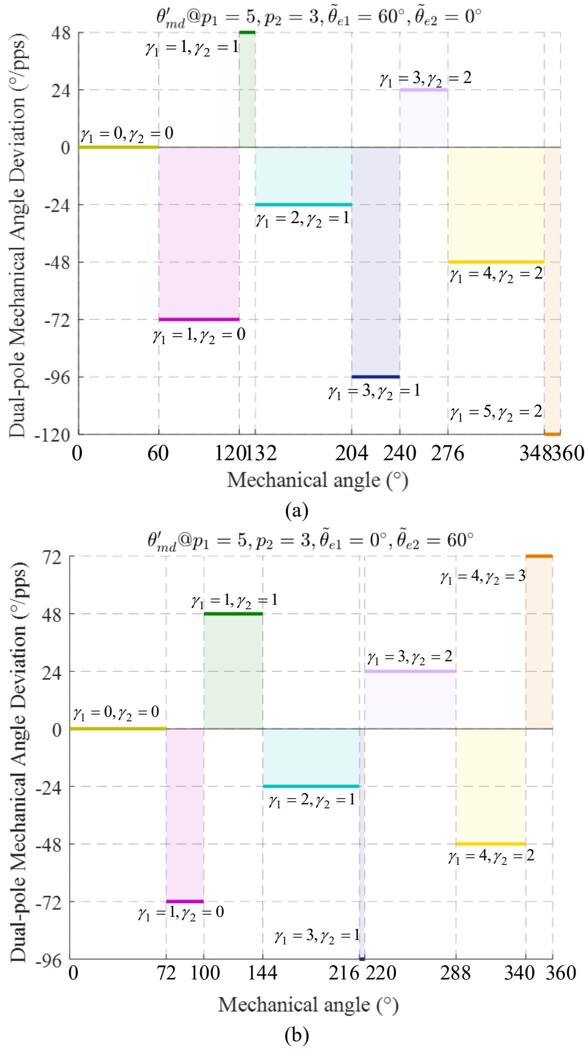

Fig. 6. The value of θ'_{md} when considering electrical angle errors. (a) The outer air gap $\tilde{\theta}_{e1}$ leads by 60°. (b) The inner air gap $\tilde{\theta}_{e2}$ leads by 60°.

B. *Observed Mechanical Position Correction and Its Error*

From the above analysis, it can be seen that the error of the dual-pole mechanical angle deviation is given by (9):

$$\tilde{\theta}_{md} = \hat{\theta}_{md} - \theta_{md} = \frac{\tilde{\theta}_{e1}}{p_1} - \frac{\tilde{\theta}_{e2}}{p_2} \tag{9}$$

For computational convenience, (3) is rectified and transformed as (10):

$$\frac{m_1 p_1}{p_2} - m_2 = \frac{1}{p_2} \tag{10}$$

or

$$m_1 - \frac{m_2 p_2}{p_1} = \frac{1}{p_1} \tag{11}$$

Equation (12) can be obtained after adding the correction coefficient $K = -m_2 p_2 \tilde{\theta}_{md}$ to the original observed mechanical position.

$$\begin{aligned}\hat{\theta}_{mc} &= \left(m_1\hat{\theta}_{e1} - m_2\hat{\theta}_{e2}\right) - m_2 p_2 \tilde{\theta}_{md} \\ &= m_1\left(\theta_{e1} + \tilde{\theta}_{e1}\right) - m_2\left(\theta_{e2} + \tilde{\theta}_{e2}\right) \\ &\quad - \left(\frac{m_2 p_2}{p_1}\tilde{\theta}_{e1} - m_2\tilde{\theta}_{e2}\right) \\ &= \theta_m + \frac{\tilde{\theta}_{e1}}{p_1}\end{aligned} \tag{12}$$

It can be seen that the corrected mechanical position error value is reduced to $\tilde{\theta}_{e1} / p_1$.

Similarly, when the correction coefficient is set to $K = -m_1 p_1 \tilde{\theta}_{md}$

$$\hat{\theta}_{mc} = \theta_m + \frac{\tilde{\theta}_{e2}}{p_2} \tag{13}$$

The corrected mechanical position error value is reduced to $\tilde{\theta}_{e2} / p_2$.

It can be observed that once $\tilde{\theta}_{md}$ is determined and the correction coefficient is incorporated, the observed mechanical positioning accuracy will be significantly enhanced, being solely influenced by the electrical angle error of one-side air gap, while remaining independent of both the m value and the electrical angle error of the other air gap. Critically, the correction method eliminates the need to distinguish between DC and AC components within the electrical angle observation errors, thereby providing effective suppression of position errors even under non-ideal conditions such as magnetic distortion or parameter variations.

Taking p_1=5 and p_2=3 as an example, m_1=2 and m_2=3 can be obtained from (3). As shown in Figs. 5(a) and 6, the intervals between adjacent θ_{md} values are uniformly 24°. By setting the tolerance to half of the angle interval between adjacent θ_{md} values, a bidirectional tolerance interval can be established, enabling accurate identification of the true θ_{md} value during operation. Thus, the tolerance can be set to 12°.

The value of $\tilde{\theta}_{md}$ can be determined by the observed $\hat{\theta}_{md}$ and the value of θ_{md} with $\left|\tilde{\theta}_{md}\right|$<12° obtained by the above distribution. This value is used to correct the observed mechanical position. Specifically, for p_1=5 and p_2=3, the correction condition is defined as (14):

$$\left|\frac{\tilde{\theta}_{e1}}{p_1} - \frac{\tilde{\theta}_{e2}}{p_2}\right| < 12° \tag{14}$$

The matching relationship between the inner and outer air gap electrical angle errors is shown in Fig. 7. When the inner and outer air gap position errors are located in the grid area in the figure, the correction conditions can be satisfied.

In practice, the zero point of the position error of the inner and outer air gap can be used as the origin to make a square graph, and the allowable boundary of the electrical angle observation error can be determined as (15):

$$\left|\tilde{\theta}_{e1}\right| = \left|\tilde{\theta}_{e2}\right| \tag{15}$$

Combining (14) and (15) and solving them simultaneously, one can obtain $\tilde{\theta}_{e1} = \pm 22.5°$, $\tilde{\theta}_{e2} = \pm 22.5°$.

Notably, adjusting the pole-pair combination in the motor alters the spatial distribution pattern and numerical spacing intervals of the mechanical angle displacement θ_{md}. Consequently, changes in the pole-pair combination necessitate reconfiguration of the tolerance threshold, leading to corresponding adjustments in the permissible bounds for electrical angle estimation errors. Although the permissible bounds depend on the pole-pair number, the fundamental mathematical derivation underlying this method remains invariant. Therefore, the method is applicable to motor systems with varying pole-pair combinations.

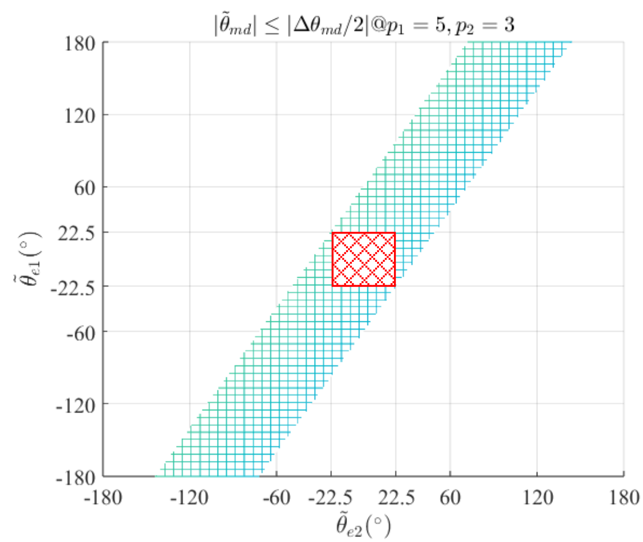

Fig. 7. The error boundary of $\tilde{\theta}_{md}$.

Existing studies demonstrate that electrical angle errors typically remain below 10° [27]-[30], while the proposed correction method merely requires confining the sensorless electrical angle error within a range of 22.5°, indicating that this condition is less stringent. The range shown in the square of Fig. 7 can be changed to a rectangular range even if the electrical angle error of one side exceeds 22.5°. It only needs to meet the correction conditions within the grid range.

IV. Experimental Verification and Result Analysis

The proposed mechanical position correction method is experimentally validated on a 0.75 kW DDCM. The experimental platform is shown in Fig. 8. Table I presents parameters of the DDCM.

The experimental platform acquires the rotor angle displacement signal in real-time via the Tamagawa TS2620N21E11 resolver, with data processed by an AD2S1210 decoder IC featuring 16-bit absolute resolution. This decoder supports the serial peripheral interface (SPI) communication protocol. The system master controller employs the TMS320F28335 digital signal processor (DSP). The inner and the outer motor drive subsystems utilize a galvanically isolated, independent power supply architecture.

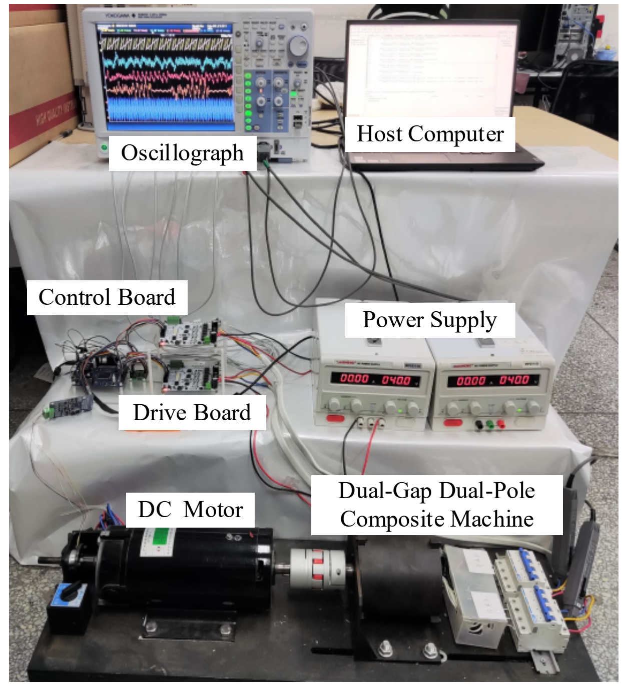

Fig. 8. Experimental platform.

TABLE I
MAIN PARAMETERS OF MOTOR

Parameters	Value	Parameters	Value
External motor rated power, P_{N1}/W	500	External motor rotor flux linkage, ψ_{s1}/Wb	0.0227
Internal motor-rated power, P_{N2}/W	250	Inner motor rotor flux linkage, ψ_{s2}/Wb	0.0284
Bus voltage, U_{dc}/V	48	External motor phase resistance, R_{s1}/Ω	0.0591
Rated torque, T_N/(N·m)	2.9756	Internal motor phase resistance, R_{s2}/Ω	0.5741
Rated speed, n_N/(r·min^{-1})	2000	External motor d-axis inductance, L_{d1}/mH	0.3564
Switching frequency, f_c/kHz	5	External motor q-axis inductance, L_{q1}/mH	0.6829
Number of pole-pairs of outer motor, p_1	5	Inner motor d-axis inductance, L_{d2}/mH	0.4328
Number of pole-pairs of inner motor, p_2	3	Inner motor q-axis inductance, L_{q2}/mH	1.0131

The mechanical speed of the DDCM is set to be 300 r·min^{-1}. In Fig. 9, $\hat{\theta}_{e1}$ is the observed value of the outer air gap electrical angle, $\hat{\theta}_{e2}$ is the observed value of the inner air gap electrical angle, $\hat{\theta}_{m}$ is the observed value of the mechanical position, $\tilde{\theta}_{e1}$ is the outer air gap electrical angle error, and $\tilde{\theta}_{e2}$ is the inner air gap electrical angle error.

When the electrical angle error of the inner and outer air gaps is considered, the solved mechanical position error depends on the fit between the inner and outer air gaps. When the fit between them is poor, the solved mechanical position error fluctuates dramatically.

As shown in Fig. 9, the outer air gap electrical angle error ranges from −11° to +4.6°, while the inner air gap error ranges from −6.4° to +0.6°. The mechanical angle position error reaches up to 24° with significant error fluctuation.

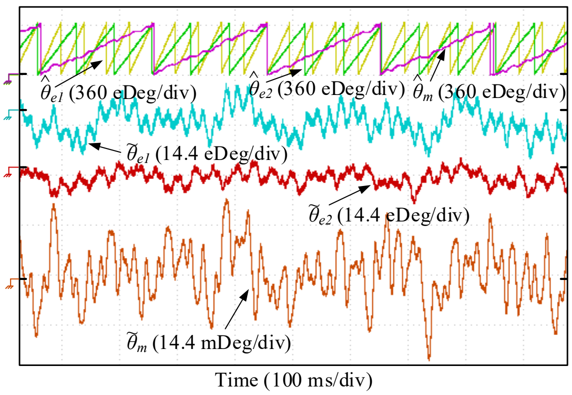

Fig. 9. Electrical position error and solving mechanical position error.

As shown in Fig. 10, when the observed mechanical position error $\tilde{\theta}_{\mathrm{m}}$ is corrected by (12), its value is one of the pole-pairs of the angle error of the outer air gap. Its value before correction is −11.5° to +14.5°, but its value after correction is −1.7° to +0.7°. The observed mechanical position error is reduced by an order of magnitude, and the fluctuation is greatly reduced.

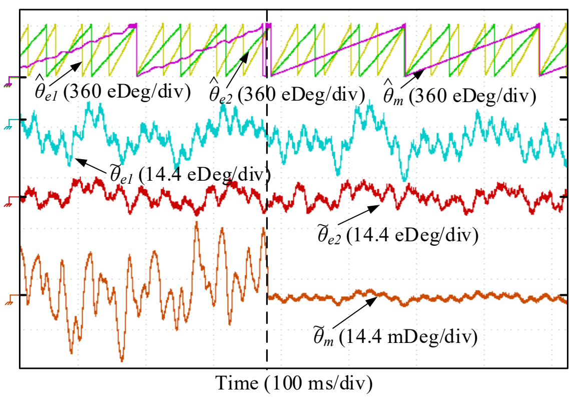

Fig. 10. The observed mechanical position error is corrected to one of the pole-pairs of the angle error of the outer air gap.

As shown in Fig. 11, when the observed mechanical position error $\tilde{\theta}_{\mathrm{m}}$ is corrected by (13), its value is one of the pole-pairs of the angle error of the inner air gap. Its value is −17.7° to +10.6°, but its value after correction is −1.9° to +0.8°. The same observed mechanical position error and fluctuation are greatly reduced.

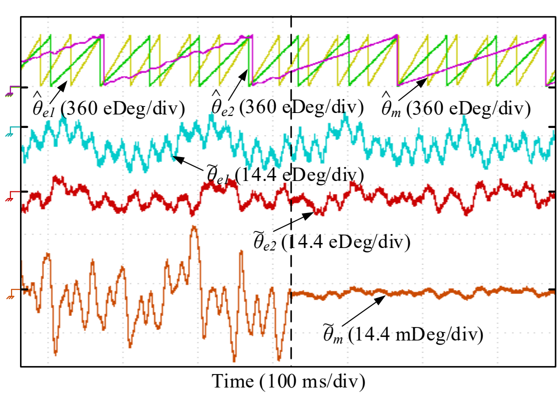

Fig. 11. The observed mechanical position error is corrected to one of the pole-pairs of the angle error of the inner air gap.

In order to prove that the corrected solved mechanical position error is only affected by the electrical position error on one side, the solved mechanical position error is observed after artificially superimposing the electrical position error in the inner and outer air gaps, respectively, while the motor is running. A sinusoidal position error with a frequency of 25 Hz and an amplitude of 5° was added to the outer air gap, and a sinusoidal position error with a frequency of 15 Hz and an amplitude of 5° was added to the inner air gap.

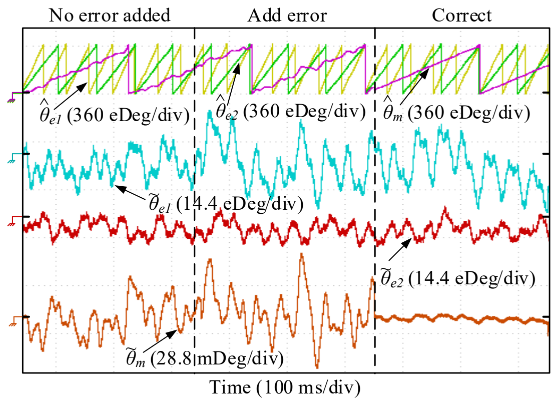

Fig. 12. Position error is added to the outer air gap, and the mechanical position error is calibrated to the electrical angle error of the outer air gap divided by the corresponding number of pole-pairs.

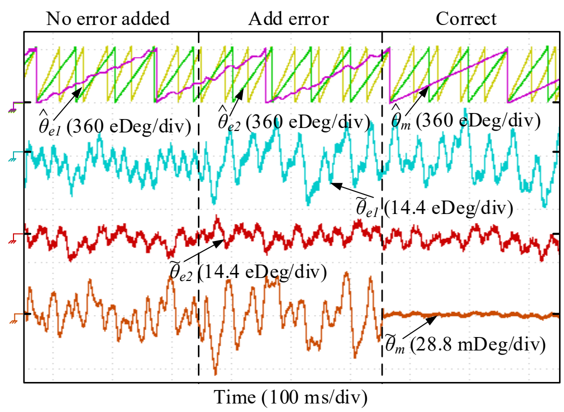

Fig. 13. Position error is added to the outer air gap, and the mechanical position error is calibrated to the inner air gap electrical angle error divided by the corresponding number of pole-pairs.

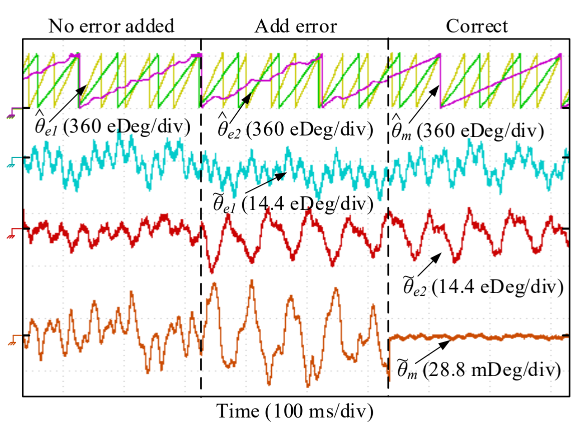

Fig. 14. Position error is added to the inner air gap, and the mechanical position error is calibrated to the outer air gap electrical angle error divided by the corresponding number of pole-pairs.

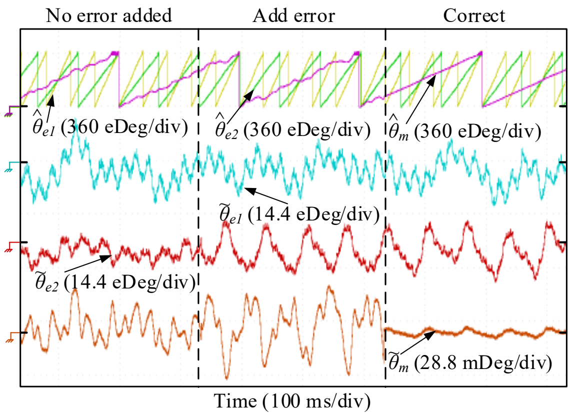

Fig. 15. Position error is added to the inner air gap, and the mechanical position error is calibrated to the inner air gap electrical angle error divided by the corresponding number of pole-pairs.

As shown in Figs. 12–15, when position errors are respectively added to inner and outer air gaps, the uncorrected observed mechanical position errors are jointly affected by the electrical angle errors of the inner and outer air gaps. When either side of the electrical angle error changes, it will cause a significant fluctuation in the observed mechanical position error.

As shown in Figs. 12 and 14, after the mechanical position error is corrected to one pole-pair of the outer air-gap electrical angle error, the error is corrected to the range of −2.0° to +1.6° (Fig. 12) and −1.7° to +0.7° (Fig. 14). Comparative experiments show that, after a sinusoidal position error is introduced into the inner air gap, the amplitude of the system's mechanical position error corrected via the outer air gap remains consistent with the correction result without any error added. This verifies that the corrected mechanical position error is solely governed by unilateral electrical position error.

Similarly, as shown in Figs. 13 and 15, after the mechanical position error is corrected to one pole-pair of the inner air-gap electrical angle error, the error is corrected to the range of −1.9° to +0.8° (Fig. 13) and −1.9° to +2.2° (Fig. 15). Comparative experiments show that, after a sinusoidal position error is introduced into the outer air gap, the amplitude of the system's mechanical position error corrected via the inner air gap remains consistent with the correction result without any error added, which verifies the conclusion that the corrected mechanical position error is determined solely by the unilateral electrical position error.

In summary, the observed mechanical position error after correction according to (12) and (13) is only determined by the electrical angle error on one side and is not affected by the electrical angle error on the other side.

V. Conclusion

Based on the DDCM, this paper systematically analyzes the effects of pole-pair numbers and electrical angle errors on mechanical position estimation errors of the motor and proposes a novel correction method to mitigate the position errors. This method corrects mechanical position estimation errors to electrical angle position errors within the inner or outer air-gap multiplied by the inverse of corresponding pole-pair numbers, thereby rendering mechanical position estimation errors exclusively governed by the electrical angle error of a single air-gap. This approach resolves error amplification issues induced by suboptimal pole-pair selection while eliminating amplification stemming from undesirable coupling between inner and outer air-gap errors, concurrently suppressing both DC and AC components of mechanical position estimation errors.

This paper presents the correction method's applicability constraints, demonstrating its low sensitivity to electrical angle estimation errors. It can be deployed in conventional sensorless controls, providing theoretical and technical support for position estimation in high-precision servo drives and integrated robotic systems.

References

[1] W. Q. Lu, B. Tang, and K. Y. Ji *et al.*, "A New Load Adaptive Identification Method based on an Improved Sliding Mode Observer for PMSM Position Servo System," *IEEE Trans. on Power Electr.*, vol. 36, no. 3, pp. 3211–3223, Mar. 2021.

[2] B. Tang, W. Q. Lu, and B. Yan *et al.*, "A Novel Position Speed Integrated Sliding Mode Variable Structure Controller for Position Control of PMSM," *IEEE Trans. on Ind. Electron*, vol. 69, no. 12, pp. 12621–12631, Dec. 2022.

[3] S. B. Li, Y. X. Xu, and W. T. Zhang *et al.*, "A Novel Two-phase Mode Switching Control Strategy for PMSM Position Servo Systems with Fast-response and High-precision," *IEEE Trans. on Power Electron*, vol. 38, no. 1, pp. 803–815, Jan. 2023.

[4] F. Zare, A. Keyvannia, and Z. Nasiri-Gheidari, "Presentation of a Novel Variable Reluctance Tubular Resolver," *IEEE Trans. on Ind. Electron*, vol. 69, no. 12, pp. 13773–13780, Dec. 2022.

[5] M. Dalboni, and A. Soldati, "Absolute Two-tracked Optical Rotary Encoders based on Vernier Method," *IEEE Trans. on Instrum. and Meas*, vol. 72, pp. 1–12, Jan. 2023.

[6] H. Oh, K. Y. Song, and K. Y. Cho *et al.*, "Initial Rotor Position Detecting Algorithm of PM Synchronous Motor Using Incremental Encoder," in *Proc. of 2013 IEEE ECCE Asia Downunder*, Melbourne, VIC, Australia, 2013, pp. 681–686.

[7] D. Fernandez, D. Fernandez, and M. Martinez *et al.*, "Resolver Emulation for PMSMs Using Low Cost Hall-effect Sensors," *IEEE Trans. on Ind Appl*, vol. 56, no. 5, pp. 4977–4985, Sept.-Oct. 2020.

[8] K. C. Kim, "Analysis on the Charateristics of Variable Reluctance Resolver Considering Uneven Magnetic Fields," *IEEE Trans. on Magn*, vol. 49, no. 7, pp. 3858–3861, Jul. 2013.

[9] S. S. Kuruppu, S. G. Abeyratne, and S. Hettiarachchi, "Modeling and Detection of Dynamic Position Sensor Offset Error in PMSM Drives," *IEEE Access*, vol. 11, pp. 36741–36752, 2023.

[10] X. Ge, Z. Q. Zhu, and R. Ren *et al.*, "A Novel Variable Reluctance Resolver with Nonoverlapping Tooth-coil Windings," *IEEE Trans. on Energy Convers*, vol. 30, no. 2, pp. 784–794, Jun. 2015.

[11] S. Chi, Z. Zhang, and L. Y. Xu, "Sliding-mode Sensorless Control of Direct-drive PM Synchronous Motors for Washing Machine Applications," *IEEE Trans. on Ind Appl*, vol. 45, no. 2, pp. 582–590, Mar-Apr. 2009.

[12] Q. Wang, S. H. Wang, and C. H. Chen, "Review of Sensorless Control Techniques for PMSM Drives," *IEEJ Trans. on Electr. and Electron. Engineering*, vol. 14, no. 10, pp. 1543–1552, Oct. 2019.

[13] S. K. Sul, and S. Kim, "Sensorless Control of IPMSM: Past, Present, and Future," *IEEJ J. of Ind. Appl.*, vol. 1, no. 1, pp. 15–23, 2012.

[14] G. L. Wang, M. Valla, and J. Solsona, "Position Sensorless Permanent Magnet Synchronous Machine Drives—A Review," *IEEE Trans. on Ind. Electron*, vol. 67, no. 7, pp. 5830–5842, Jul. 2020.

[15] Y. C. Kwon, S. K. Sul, and N. A. Baloch *et al.*, "Design and Control of IPMSM Sensorless Drive for Mechanical Rotor Position Estimation Capability," *IEEE J. of Emerg. and Sel. Topics in Power Electron*, vol. 2, no. 2, pp. 152–158, Jun. 2014.

[16] Y. C. Kwon, S. K. Sul, and N. A. Baloch *et al.*, "Design, Modeling, and Control of an IPMSM with an Asymmetric Rotor and Search Coils for Absolute Position Sensorless Drive," *IEEE Trans. on Ind Appl*, vol. 52, no. 5, pp. 3839–3850, Sept.-Oct. 2016.

[17] Y. C. Kwon, S. K. Sul, and N. A. Baloch *et al.*, "Improved Design of IPMSM for Sensorless Drive with Absolute Rotor Position Estimation Capability," *IEEE Trans. on Ind Appl*, vol. 52, no. 2, pp. 1441–1451, Mar.-Apr. 2016.

[18] R. G. Ni, S. Z. Gu, and S. X. Nie *et al.*, "Dual-gap Dual-pole Composite Machine for Mechanical Rotor Position Estimation," *IEEE Trans. on Power Electron*, vol. 36, no. 9, pp. 10481–10489, Sept. 2021.

[19] R. G. Ni, D. G. Xu, and F. Blaabjerg *et al.*, "Square-wave Voltage Injection Algorithm for PMSM Position Sensorless Control with High Robustness to Voltage Errors," *IEEE Trans. on Power Electron*, vol. 32, no. 7, pp. 5425–5437, Jul. 2017.

[20] G. Q. Zhang, G. L. Wang, and D. G. Xu *et al.*, "Multiple-AVF Cross-feedback-network-based Position Error Harmonic Fluctuation Elimination for Sensorless IPMSM Drives," *IEEE Trans. on Ind. Electron*, vol. 63, no. 2, pp. 821–831, Feb. 2016.

[21] B. Stumberger, G. Stumberger, and D. Dolinar *et al.*, "Evaluation of Saturation and Cross-magnetization Effects in Interior Permanent-magnet Synchronous Motor," *IEEE Trans. on Ind Appl*, vol. 39, no. 5, pp. 1264–1271, Sept.-Oct. 2003.

[22] T. F. Qiu, X. H. Wen, and F. Zhao, "Adaptive-linear-neuron-based Dead-time Effects Compensation Scheme for PMSM Drives," *IEEE Trans. on Power Electron*, vol. 31, no. 3, pp. 2530–2538, Mar. 2016.

[23] A. Saghafinia, H. W. Ping, and M. N. Uddin *et al.*, "Adaptive Fuzzy Sliding-mode Control Into Chattering-free IM Drive," *IEEE Trans. on Ind Appl*, vol. 51, no. 1, pp. 692–701, Jan.-Feb. 2015.

[24] M. H. Zhou, S. W. Cheng, and Y. Feng *et al.*, "Full-order Terminal Sliding-mode-based Sensorless Control of Induction Motor with Gain Adaptation," *IEEE J. of Emerg. and Sel. Topics in Power Electron*, vol. 10, no. 2, pp. 1978–1991, Apr. 2022.

[25] S. Decker, J. Stoß, and A. Liske *et al.*, "Online Parameter Identification of Permanent Magnet Synchronous Machines with Nonlinear Magnetics based on the Inverter Induced Current Slopes and the dq-system Equations," in *Proc. of 2019 21st European Conference on Power Electronics and Applications (EPE '19 ECCE Europe)*, Genova, Italy, 2019, pp. P.1–P.10.

[26] L. J. Wu, Z. K. Lyu, and Z. K. Chen *et al.*, "An Enhanced Sensorless Control Scheme for PMSM Drives Considering Self-inductance Asymmetry," *CES Trans. on Electr. Mach. and Sys.*, vol. 6, no. 4, pp. 384–392, Dec. 2022.

[27] G. L. Wang, Z. M. Li, and G. Q. Zhang *et al.*, "Quadrature PLL-based High-order Sliding-mode Observer for IPMSM Sensorless Control with Online MTPA Control Strategy," *IEEE Trans. on Energy Convers*, vol. 28, no. 1, pp. 214–224, Mar. 2013.

[28] G. L. Wang, H. L. Zhan, and G. Q. Zhang *et al.*, "Adaptive Compensation Method of Position Estimation Harmonic Error for EMF-based Observer in Sensorless IPMSM Drives," *IEEE Trans. on Power Electron*, vol. 29, no. 6, pp. 3055–3064, Jun. 2014.

[29] X. H. Jin, R. G. Ni, and W. Chen *et al.*, "High-frequency Voltage-injection Methods and Observer Design for Initial Position Detection of Permanent Magnet Synchronous Machines," *IEEE Trans. on Power Electron*, vol. 33, no. 9, pp. 7971–7979, Sept. 2018.

[30] R. G. Ni, Y. Q. Cai, and S. Z. Gu *et al.*, "Improved Analytical Analysis of Novel Integrated Variable Reluctance Resolver for Compact Machine Topology," *IEEE Trans. on Ind. Electron*, vol. 69, no. 12, pp. 12600–12609, Dec. 2022.

Yukun Lin was born in Shandong, China. He received the B.S. degree in electrical engineering from Qingdao University, Qingdao, China, in 2023. He is currently working toward the M.S. degree in electrical engineering in Qingdao University, Qingdao, China.

His research interests include position sensorless control in permanent magnet synchronous motors and the motor drive.

Ronggang Ni (Senior Member, IEEE) received the B.S., M.S. and Ph.D. degrees from Harbin Institute of Technology, Harbin, China, in 2010, 2012, and 2017, respectively, all in Electrical Engineering.

From 2015 to 2016, he was a Visiting Scholar at the Department of Energy Technology, Aalborg University, Denmark. In 2017, he was with the Shanghai STEP Electric Corporation, Shanghai, China. From 2018, he has been an Professor with Qingdao University, Qingdao, China. He is currently the Vice Dean of the School of Electrical Engineering. His research interests include design of electric machines for high efficiency and high power density applications, and electric drives with less sensors.

Dr. Ni is an active reviewer for IEEE sponsored conferences and several IEEE top journals.

Shengming Yang was born in Shandong, China. He received the B.S. and M.S. degrees in electrical engineering from Qingdao University, Qingdao, China, in 2021 and 2024, respectively.

His research interests include position sensorless control in permanent magnet synchronous motors.

Qingwen Deng was born in Hunan, China. She received the B.S. degree in Smart Grid Information Engineering from Chongqing University of Posts and Telecommunications in 2024. She is currently working toward the M.S. degree in electrical engineering at Qingdao University in China.

Her research interests include dual air gap compound permanent magnet motor and multiphase inverter design based on GaN.